JACS
JOURNAL OF THE AMERICAN CHEMICAL SOCIETY

COMMUNICATION

pubs.acs.org/JACS

Ratiometric Temperature Sensing with Semiconducting Polymer Dots

Fangmao Ye, Changfeng Wu, Yuhui Jin, Yang-Hsiang Chan, Xuanjun Zhang, and Daniel T. Chiu*

Department of Chemistry, University of Washington, Seattle, Washington 98195, United States

Supporting Information

ABSTRACT: This communication describes ultrabright single-nanoparticle ratiometric temperature sensors based on semiconducting polymer dots (Pdots). We attached the temperature sensitive dye—Rhodamine B (RhB), whose emission intensity decreases with increasing temperature—within the matrix of Pdots. The as-prepared Pdot-RhB nanoparticle showed excellent temperature sensitivity and high brightness because it took advantage of the light harvesting and amplified energy transfer capability of Pdots. More importantly, the Pdot-RhB nanoparticle showed ratiometric temperature sensing under a single wavelength excitation and has a linear temperature sensing range that matches well with the physiologically relevant temperatures. We employed Pdot-RhB for measuring intracellular temperatures in a live-cell imaging mode. The exceptional brightness of Pdot-RhB allows this nanoscale temperature sensor to be used also as a fluorescent probe for cellular imaging.

Temperature is a fundamental physical parameter that affects the behavior of chemical and biological systems. Accurate temperature determination is important in cells because temperature influences both equilibrium constants and biochemical reaction kinetics that range from gene expression to energy metabolism. In disease states such as cancer, malignant cells within tissues can be at an elevated temperature compared to healthy cells because of differences in cellular metabolism.[1] Thus, it is important to have techniques and devices that are capable of accurately monitoring temperature within biological systems.

Unfortunately, traditional methods based on thermocouples, albeit sensitive and accurate, cannot measure temperatures remotely within small confined spaces or at many locations simultaneously, for instance, within individual cells of a complex cellular network. Because of these constraints, optical temperature measurements—such as those based on the use of rare-earth doped materials,[2−9] quantum dot clusters,[10,11] organic dye molecule,[12] gold-CdTe nanoparticle,[13] and NIPAM based materials[14,15]—have recently attracted much attention. Optical temperature determination has the advantages of being noninvasive and inherently parallel, which makes the approach particularly suitable for microfluidic[16,17] and biological imaging experiments.[18,19]

Because of the complex cellular environment, optical temperature sensors should possess several qualities for in vivo measurements. First, the optical signal from the sensor must be bright enough to overcome background signals and autofluorescence from cellular materials. Second, the optical temperature sensor should be nontoxic to the cell, a feature that is particularly important for long-term cellular studies. And third, given the complex biochemical milieu in a physiological solution, the optical readout from the temperature sensor ideally should be ratiometric. Most current optical temperature sensing schemes, including those based on molecules (e.g., temperature sensitive fluorescent dyes[12]) and nanoparticles (e.g., quantum dots,[10,11] and nanogels[18]), are nonratiometric and rely on measuring changes in fluorescence signal at a single wavelength.

To address this need for accurate and robust optical temperature sensing, we describe a new approach to designing ultrabright ratiometric temperature sensors based on semiconducting polymer dots (Pdots).[20−22] Pdots represent a new class of fluorescent probes with dimensions that can be manipulated from a few nanometers to tens of nanometers, with a fluorescence brightness that can be orders of magnitude greater than that of organic dyes and tens of times better than that of quantum dots.[21,22] Bioconjugation and controlling the surface chemistry of Pdots had been a challenge, but we recently developed a method for conjugating a wide range of biomolecules to Pdots.[21,22] In this study, we attached the temperature sensitive dye—Rhodamine B (RhB), whose emission intensity decreases with increasing temperature—within the matrix of Pdots. The final Pdot-RhB nanoparticle showed excellent temperature sensitivity and high brightness because it took advantage of the light harvesting and amplified energy transfer capability of Pdots. More importantly, because we could choose semiconducting polymers for the Pdots with emission features that were temperature insensitive, we were able to design ratiometric temperature sensors with two emission peaks under a single wavelength excitation.

Figure 1A and 1B schematically show our approach, in which we first conjugated RhB to an amphiphilic, amino-terminated, polystyrene polymer (PS-NH_2) to form PS-RhB. We then used a nanoscale precipitation technique that blended PS-RhB with a semiconducting polymer (either poly[(9,9-dioctylfluorenyl-2,7-diyl)-*co*-(1,4-benzo-{2,1′,3}-thiadiazole)] (**PFBT**) or poly-[{9,9-dioctyl-2,7-divinylene-fluorenylene}-*alt*-*co*-{2-methoxy-5-(2-ethylhexyloxy)-1,4-phenylene}] (**PFPV**)) to form the final Pdot-RhB nanoparticle.

To ensure efficient energy transfer, RhB should be in close proximity with the semiconducting polymer. Initially, we simply tried to dope free RhB into Pdots because we thought RhB was sufficiently hydrophobic to be entrapped within the hydrophobic Pdot matrix. Contrary to our expectation, we found RhB did not partition well into the Pdot matrix. Our strategy of blending PS-RhB with the semiconducting polymer of the Pdots during the nanoscale precipitation procedure overcame this issue.

Received: March 31, 2011
Published: May 06, 2011

ACS Publications © 2011 American Chemical Society

dx.doi.org/10.1021/ja202945g | *J. Am. Chem. Soc.* 2011, 133, 8146–8149

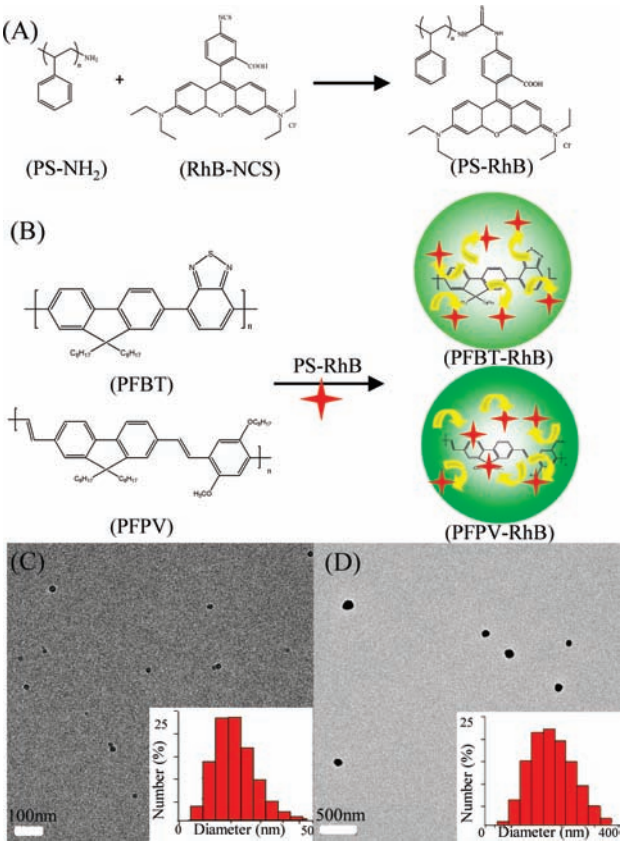

Figure 1. (A) Conjugation of RhB isothiocyanante (RhB-NCS) to an amphiphilic amino-terminated polystyrene polymer (PS-NH_2) to form PS-RhB. (B) Formation of temperature sensitive Pdot-RhB (PFBT-RhB or PFPV-RhB) by blending PS-RhB with a semiconducting polymer (either PFBT or PFPV) during nanoprecipitation. Arrows in the particle represent energy transfer from the semiconducting polymer to RhB. (C) Transmission electron microscopy (TEM) image and dynamic light scattering (DLS) measurement (histogram) of the size of PFPV-RhB. (D) TEM and DLS measurement (histogram) of the size of PFBT-RhB.

The sizes of Pdot-RhB can be tuned. The PFPV-RhB dots we made averaged 22 nm in hydrodynamic diameter (Figure 1C) while the PFBT-RhB dots were around 160 nm in hydrodynamic diameter (Figure 1D). By varying the nanoscale precipitation conditions, the molecular weight or type of semiconducting polymer, or the amount of PS-RhB blended into the Pdots, we could vary their size over a wide range. We tested blending different amounts of PS-RhB with PFBT or PFPV and found 10 wt % worked best in terms of colloidal stability and the final temperature sensitivity and brightness of the nanoparticles.

Our approach relied on efficient fluorescence resonance energy transfer (FRET) from Pdot to RhB. For this to occur, the emission of donor had to overlap well with the absorption of acceptor. Although we explored the performance of several semiconducting polymers, we found PFPV and PFBT offered the best result: they were very bright. The quantum yield of PFBT-RhB was measured to be 0.3 which is equal to bare PFBT Pdot.[21,22] For PFPV-RhB, the quantum yield is 0.1 which is about 2 times higher than that for bare PFPV Pdot. The FRET efficiency between PFBT/PFPV-RhB is up to 60%, and they had a linear response over the physiologically relevant temperature range and suitable spectral features for use as a ratiometric temperature sensor.

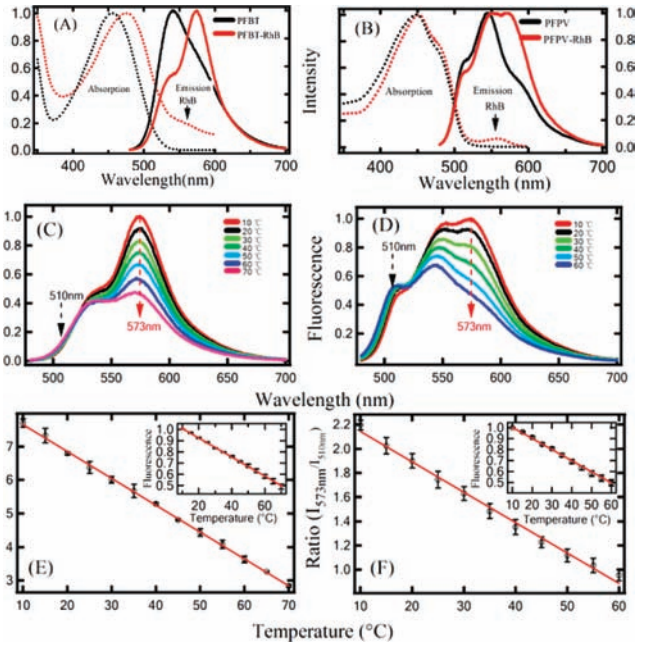

Figure 2. Absorption (dashed) and emission (solid) spectra for (A) PFBT and PFBT-RhB Pdots and (B) PFPV and PFPV-RhB Pdots. The arrow shows absorption peak of RhB in the Pdots. Fluorescence spectra of (C) PFBT-RhB and (D) PFPV-RhB at different temperatures. The ratio of the 573-nm over the 510-nm peaks as a function of temperature were plotted for (E) PFBT-RhB and (F) PFPV-RhB; the insets plot the normalized intensities of the 573-nm peak versus temperature, showing the linear decrease in fluorescence intensity as a function of temperature. The error bars in (E) and (F) represent standard deviation of three independent measurements. To obtain the emission spectra, 450-nm light was used to excite all Pdots.

Both PFPV and PFBT had a peak emission around 540 nm, which overlapped well with the absorption peak of RhB. The close proximity of RhB to the semiconducting polymer when embedded within the Pdot matrix also facilitated energy transfer. Most importantly, both PFPV and PFBT were efficiently excited at 450 nm, a wavelength region where RhB was poorly excited. Furthermore, the emissions from Pdot and RhB could be spectrally separated, and because Pdot emission was temperature insensitive while RhB emission was highly temperature dependent, we used Pdot emission as an internal reference to construct a ratiometric temperature sensor.

Figure 2A shows the absorption (dashed) and emission (solid) spectra of PFBT (black) and PFBT-RhB (red) Pdots at room temperature. Compared to pure PFBT Pdots, the absorption spectrum of PFBT-RhB had an additional small absorption peak at 555 nm that was accompanied by a small, ~ 10-nm red shift of the main PFBT absorption peak. The small absorption peak that appeared at 555 nm was from RhB. PFBT-RhB Pdots exhibited two emission peaks—a "hump" at around 540 nm and a stronger emission peak at 573 nm. The latter peak corresponded to the emission of RhB, derived from the excellent energy transfer from PFBT to RhB when excited at 450 nm; the small hump around 540 nm was the residual fluorescence from PFBT.

Figure 2B shows the absorption and emission spectra of PFPV and PFPV-RhB Pdots at room temperature. The PFPV and PFPV-RhB Pdots showed similar behavior as the PFBT and PFBT-RhB Pdots. The emission spectrum of PFPV-RhB was slightly different than that of PFBT-RhB, with a "hump" at

dx.doi.org/10.1021/ja202945g |J. Am. Chem. Soc. 2011, 133, 8146–8149

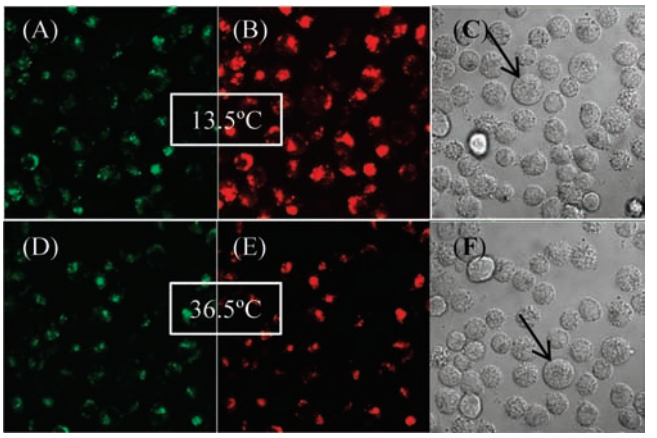

Figure 3. Confocal microscopy images of HeLa cells labeled with PFBT-RhB at λ_{exc} = 458 nm at 13.5 °C (A–B) and 36.5 °C (D–E); their corresponding bright-field images are shown in (C) and (F). The green channels shown in (A) and (D) were produced by integrating the spectral region from 507 to 518 nm, while the red channels shown in (B) and (E) were from 571 to 582 nm. The scale bar is 20 μm. The arrows in (C) and (F) point to the same cell whose integrated spectra were shown in Figure S1 (Supporting Information).

510 nm and two closely spaced emission peaks at 540 and 573 nm. As with the PFBT-RhB Pdots, we observed excellent energy transfer from PFPV to RhB.

We next investigated the temperature sensitivity of PFPV-RhB and PFBT-RhB Pdots. Figure 2C and 2D show the fluorescence spectra of the Pdot-RhB nanoparticles as a function of temperature when excited at 450 nm. The right dashed arrow (red) shows the emission peak of RhB at 573 nm, which was temperature dependent, while the left dashed arrow (black) points to the temperature-insensitive emission at 510 nm from the semiconducting polymer.

To quantitatively determine whether the temperature-dependent changes in the emission spectra could be used for accurate temperature sensing, we plotted the change in the normalized fluorescence intensity of the 573-nm peak and the ratio of the 573-nm to 510-nm peak as a function of temperature (Figure 2E and 2F). For PFBT-RhB, we found 10–70 °C was the range over which fluorescence intensity changed linearly with temperature (R^2 = 0.999). For PFPV-RhB, the linear range was 10–60 °C (R^2 = 0.998). Both temperature-sensitive Pdots showed a fluorescence-intensity change of ~1% per °C. Figure 2E and 2F plot the ratio of I_{573nm}/I_{510nm}, from which we obtained a linear fit with an R^2 of 0.999 for PFBT-RhB and an R^2 of 0.996 for PFPV-RhB. It should be noted that the ratiometric sensing range (10–70 °C) of Pdot-RhB is much wider than those of NIPAM-based material.[14,15]

Next, we applied Pdot-RhB for measuring intracellular temperatures in a live-cell imaging mode. Here, we introduced PFBT-RhB (1 nM in cell-culture media) into live HeLa cells via endocytosis without any additional reagents. After cellular uptake, we washed the cells with PBS buffer to remove free Pdots in solution and on the cell surface. The temperature of the cell solution was controlled using a heating stage on the microscope. Independently, the temperature of the cell solution was determined with a thermocouple probe immersed in the solution.

Figure 3 shows the confocal fluorescence images of HeLa cells after the endocytosis of PFBT-RhB at 13.5 °C (A–B) and 36.5 °C (D–E). The green channels (panel A and D) were obtained by integrating the spectral region from 507 to 518 nm, and the red channels (panels B and E) were acquired by integrating the fluorescence signals from 571 to 582 nm. Their bright field images are shown in panels C and F, respectively. The intensity of the red channel in panel B (13.5 °C) is higher than that in panel E (36.5 °C) as expected. Figure S1 plots the fluorescence intensity as a function of channel wavelength of the cell pointed to with an arrow in panels C and F at 13.5 and 36.5 °C.

Because the green and red channels collected fluorescence intensity over a range of 11 nm, we integrated the fluorescence spectrum shown in Figure 2C into 11 nm bins, from which we plotted a new calibration plot (Figure S2) that we used to obtain the cell temperatures reported by the PFBT-RhB Pdots.

The average cell temperature reported by PFBT-RhB was 13.2 ± 0.9 °C (40 cells) for the 13.5 °C cell solution (measured with the thermocouple) and 35.7 ± 1.8 °C (40 cells) for the 36.5 °C cell solution. The temperatures reported by PFBT-RhB and the thermocouple are in good agreement, especially given the thermocouple has an error of at least ±0.5 °C.

In conclusion, we believe Pdot-RhB is an excellent nanosensor for local temperature. It offers the high brightness of Pdots; is inherently robust because it is a ratiometric sensor; and has a linear temperature sensing range that matches well with the physiologically relevant temperatures. The exceptional brightness of a Pdot-RhB allows this nanoscale temperature sensor to be used also as a fluorescent probe for cellular imaging. Together with our recent advances at controlling specific cellular targeting of Pdots[21,22] and the fact that the size of Pdots can be tuned (e.g., ~20 and 160 nm as reported here), we believe Pdot-RhB will become a useful tool for highly parallelized and spatiotemporally resolved temperature measurements in cells and tissues.

■ ASSOCIATED CONTENT

Supporting Information. Information of PS-RhB synthesis, Pdot preparation and characterization and cell culture, labeling, and Figures S1, S2, and S3. This material is available free of charge via the Internet at http://pubs.acs.org.

■ AUTHOR INFORMATION

Corresponding Author
chiu@chem.washington.edu

■ ACKNOWLEDGMENT

This work was supported by the National Institutes of Health (NS 062725 and CA147831) and the National Science Foundation (CHE-0844688).

■ REFERENCES

(1) DeBerardinis, R. J.; Lum, J. J.; Hatzivassiliou, G.; Thompson, C. B. *Cell metabolism* **2008**, *7*, 11–20.
(2) Borisov, S.; Klimant, I. *J. Fluor.* **2008**, *18*, 581–589.
(3) Peng, H.-S.; Huang, S.-H.; Wolfbeis, O. *J. Nanopart. Res.* **2010**, *12*, 2729–2733.
(4) Peng, H.; Stich, M. I. J.; Yu, J.; Sun, L. n.; Fischer, L. H.; Wolfbeis, O. S. *Adv. Mater.* **2010**, *22*, 716–719.
(5) Yu, J.; Sun, L.; Peng, H.; Stich, M. I. J. *J. Mater. Chem.* **2010**, *20*, 6975–6981.
(6) Berthou, H.; Jogensen, C. K. *Opt. Lett.* **1990**, *15*, 1100–1102.
(7) Maurice, E.; Monnom, G.; Ostrowsky, D. B.; Baxter, G. W. *Appl. Opt.* **1995**, *34*, 4196–4199.

(8) Scholl, M. S.; Trimmier, J. R. *J. Electro. Soc.* **1986**, *133*, 643–648.
(9) Sun, T.; Zhang, Z. Y.; Grattan, K. T. V.; Palmer, A. W. *Rev. Sci. Instrum.* **1997**, *68*, 3447–3451.
(10) Biju, V.; Makita, Y.; Sonoda, A.; Yokoyama, H.; Baba, Y.; Ishikawa, M. *J. Phys. Chem. B* **2005**, *109*, 13899–13905.
(11) Han, B.; Hanson, W.; Bensalah, K.; Tuncel, A.; Stern, J.; Cadeddu, J. *Ann. Biomed. Eng.* **2009**, *37*, 1230–1239.
(12) Chen, Y. Y.; Wood, A. W. *Bioelectromagnetics* **2009**, *30*, 583–590.
(13) Lee, J.; Govorov, A. O.; Kotov, A. N. *Angew. Chem., Int. Ed.* **2010**, *44*, 7439–7442.
(14) Chen, C.-Y.; Chen, C.-T. *Chem. Commun.* **2011**, *47*, 994–996.
(15) Wu, T.; Zou, G.; Hu, J.; Liu, S. *Chem. Mater.* **2009**, *21*, 3788–3798.
(16) Ross, D.; Gaitan, M.; Locascio, L. E. *Anal. Chem.* **2001**, *73*, 4117–4123.
(17) Samy, R.; Glawdel, T.; Ren, C. L. *Anal. Chem.* **2007**, *80*, 369–375.
(18) Gota, C.; Okabe, K.; Funatsu, T.; Harada, Y.; Uchiyama, S. *J. Am. Chem. Soc.* **2009**, *131*, 2766–2767.
(19) Vetrone, F.; Naccache, R.; Zamarron, A.; Juarranz de la Fuente, A.; Sanz-Rodriguez, F.; Martinez Maestro, L.; Martin Rodriguez, E.; Jaque, D.; Garcia Sole, J.; Capobianco, J. A. *ACS Nano* **2010**, *4*, 3254–3258.
(20) Wu, C.; Bull, B.; Szymanski, C.; Christensen, K.; McNeill, J. *ACS Nano* **2008**, *2*, 2415–2423.
(21) Wu, C.; Jin, Y.; Schneider, T.; Burnham, D. R.; Smith, P. B.; Chiu, D. T. *Angew. Chem., Int. Ed.* **2010**, *49*, 9436–9440.
(22) Wu, C.; Schneider, T.; Zeigler, M.; Yu, J.; Schiro, P. G.; Burnham, D. R.; McNeill, J. D.; Chiu, D. T. *J. Am. Chem. Soc.* **2010**, *132*, 15410–15417.